Science Fund of the Republic of Serbia

Grant Agreement No.: 7750824

Call: IDEJE

Hybrid Integrated Satellite and Terrestrial Access Network

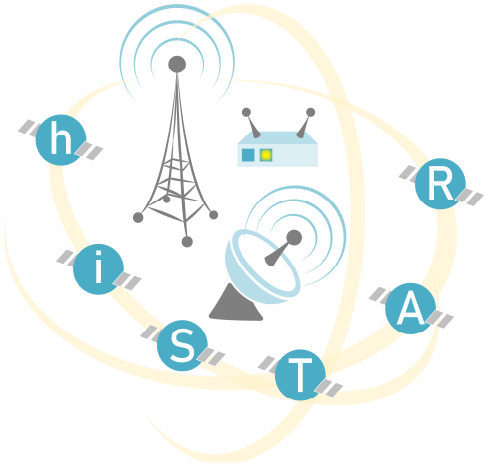

D2.3: Reliability analysis of 5G/Sat hybrid network

Work package	WP 2
Subactivity	T2.2
Due date	31.12.2023.
Submission date	15.01.2024.
Deliverable lead	Goran Đorđević
Version	1.0
Authors	Goran Đorđević, Predrag Ivaniš, Vesna Blagojević, Srđan Brkić
Reviewers	Dejan Drajić, Zoran Čiča

Document Revision History

Version	Date	Description of change	List of contributor(s)
V0.1	02.01.2024.	Document created	Goran Đorđević
V0.2	04.01.2024.	Sections 1 and 2 added	Predrag Ivaniš
V0.3	08.01.2024.	Section 3 added	Vesna Blagojević
V0.4	10.01.2024.	1st version of D2.3	Predrag Ivaniš
V0.5	12.01.2024.	2nd version of D2.3	Srđan Brkić
V1.0	15.01.2024.	Final deliverable completed	Goran Đorđević

COPYRIGHT NOTICE

ACKNOWLEDGMENT

Science Fund of the Republic of Serbia

This deliverable has been written in the context of hi-STAR project who has received funding from the Science Fund of the Republic of Serbia, Programme IDEJE under grant agreement n° 7750284.

EXECUTIVE SUMMARY

The hi-STAR project addresses integration of non-terrestrial networks with terrestrial 5G network that is in focus during the design of the next generation wireless networks. The project's main goal is to develop flexible framework for integrated terrestrial 5G and Low-Earth-Orbit (LEO) satellite networks. One of the first steps toward the framework design and implementation is defining the network architecture of the overall user access to services where user terminal has the ability to access two different RATs (Radio Access Technologies) - terrestrial and satellite.

This deliverable is a result of the work done in the context of WP2 Subtask T2.2 (Reliability analysis of integrated terrestrial and satellite links). We briefly presented the outage analysis of the hybrid integrated satellite-terrestrial communication systems. First, we discussed the case where the reliability of the system is increased by using the cooperative relaying, and the analysis takes into account the system geometry and realistic channel parameters. Finally, we present a novel framework for designing decoders, for Low-Density Parity-Check (LDPC) codes, which surpasses the frame error rate performance of Belief-Propagation (BP) decoding. Its key component is the adaptation method, based on the genetic optimization algorithm.

TABLE OF CONTENTS

LIST OF FIGURES

LIST OF TABLES

ABBREVIATIONS

5G	Fifth generation
AD-GDBF	Adaptive Diversity Gradient-Descent Bit Flipping
ARQ	Automatic Repeat reQuest
AWGN	Additive White Gaussian Noise
BCH	Bose–Chaudhuri–Hocquenghem
BP	Belief-Propagation
CDF	Cumulative Distribution Function
CSI	Channel State Information
DNN	Deep Neural Network
FAID	Finite Alphabet Iterative Decoding
FEC	Forward Error Correction
gAD-GDBF	Generalized Adaptive Diversity Gradient-Descent Bit Flipping
GDBF	Gradient Descent Bit-Flipping
ISBF	Information Storage Bit Flipping
IoT	Internet of Things
LDPC	Low-Density Parity Check
LEO	Low-Earth-Orbit
LOS	Line-of-Sight
ML	Maximum Likelihood
MRC	Maximum Ratio Combining
MTU	Master Terminal Unit
PB	Power Beacon
PDF	Probability Density Function
PGDBF	Probabilistic Gradient Descent Bit-Flipping
QoS	Quality of Service
RAT	Radio access technologies
RTU	Remote Terminal Unit
RWP	Random Waypoint
SNR	Signal-to-Noise Ratio
SWIPT	Simultaneous information and power transfer
UAV	Unmanned Aerial Vehicles
UT	User Terminal
WP	Work Package
WSN	Wireless Sensor Networks

SECTION 1 - INTRODUCTION

A major technical challenge is designing future wireless communication networks that will support a range of applications and services. Contemporary wireless networks, such as the fifth generation (5G) mobile networks should enable high data rate demands, high reliability, strong security, low latency, and energy consumption, as well as a high density of user terminals. Recently, huge efforts had been made to valorize unique characteristics of non-terrestrial networks, including wide coverage, multicast capabilities, and interoperability with terrestrial networks. The integration of satellite segment with terrestrial 5G is essential in enhancing mobile broadband, and in supporting massive machine-type communications.

The Deliverable D2.3 summarizes the continued work carried out within WP2 subtask T.2.2. In the above subtask the goal is to ensure higher reliability of integrated terrestrial network and mobile satellite LEO link. User's mobility leads to channel instability and potentially to deep-fade time intervals, in which signal strength drops below threshold required for communication. Since satellite links have large propagation delay, Automatic Repeat request (ARQ) procedures are not optimal solution to address this problem, since acknowledgements from the opposite side arrive with significant delay, which leads to very large retransmission buffering requirements at the transmitting side. To mitigate this problem, Forward Error Correction (FEC) should be applied to reconstruct information frames, lost during deep-fade events. We concentrated on a code selection study, with goal to measure performance of different code families under realistic fade models, applicable for terrestrial and satellite channels. On the other hand, we have analyzed techniques suitable for combining satellite and terrestrial links.

This deliverable is structured as follows. In Section 2 we have investigated the possibility to apply cooperative relaying in integrated satellite-terrestrial network, with the goal to increase reliability of the data transmission. The performance analysis is given for realistic channel models which are usually used to describe propagation in satellite and terrestrial links. The analytical results are verified by using previously developed simulator, described in D2.1. In Section 3, we present the performance analysis of the wirelessly powered terrestrial network employing power beacon node. We considered two scenarios employing relaying and unmanned aerial vehicles, important for IoT applications in industrial and emergency systems. The outage probability expressions are derived and reliability of the transmission is improved. The performance analysis of spectrally efficient cognitive wirelessly powered system with mobile end user, applicable for IoT systems, is also performed. Section 4 presents novel algorithm for iterative decoding of linear block codes, which provides superior performance and reduced complexity when compared with state-of-the art algorithms. The algorithm can be used for regular or irregular LDPC codes, as well as for the other linear codes. The frame error rate results are presented for LDPC codes that are used in terrestrial 5G network, and it was shown that the generalized algorithm can be applied for decoding of BCH codes, implemented in DVB-S2 standard in satellite part of the network. Section 5 concludes the document.

SECTION 2 – SATELLITE-TERRESTRIAL SYSTEMS WITH SELECTION RELAYING

In this section, we present the outage probability analysis of the hybrid integrated satellite-terrestrial communication systems, where the reliability of the system is increased by using the cooperative relaying.

It is well known that cooperative relaying techniques can increase the system performance of terrestrial wireless networks [1]. The application of cooperation techniques in integrated satellite-terrestrial systems is analyzed in [2], where it is assumed that terrestrial relays are applied. In [3], the outage probability analysis is presented for two cooperation strategies, for the case when the satellite-terrestrial links are subject to shadowed Rician fading, while the terrestrial link suffers from the Nakagami-*m* fading. However, the outage probability expressions were not presented in the closed form, and the system geometry was not considered.

The closed-form expressions for the outage probabilities are presented in the paper [4], for the integer-valued fading parameters. However, the results are presented for the case when two remote terrestrial users communicate with each other via an LEO mega constellation, and terrestrial, aerial, or satellite relays forward the information broadcasted by the satellite to the other satellite.

In this section, we consider the case where terrestrial relays forward the information broadcasted by the satellite to the final destination, as proposed in [3]. The main contribution is exact closed-form expression for the outage probability, obtained in polynomial-exponential form for the integer-valued fading parameters. The derived expressions are general and applicable to a transmission system with arbitrary chosen signal-to-noise power ratio regime, LEO satellite orbits and terrestrial and satellite link budgets.

2.1. SYSTEM AND CHANNEL MODEL

The system model of the land mobile satellite - terrestrial system with cooperative relaying is illustrated in Fig. 1. The signal with power P_S is sent from the source S both to destination D and relay R, and the relay sends a signal with power P_R to the destination. The noise power at the destination and at the relay is equal to σ^2. Following three communication links can be identified:

- The satellite-terrestrial link between the source S and the destination D, denoted as S-D, with the instantaneous signal-to-noise (SNR) at the relay [4]:

$$\gamma_1(t) = \frac{P_S}{\sigma^2 d_{SD}^{n_{SD}}} |h_1(t)|^2 = \overline{\gamma}_1 |h_1(t)|^2, \quad (1)$$

  where h_1 denotes the channel gain between the source and the destination, d_{SD} denotes its distance, and n_{SD} is the corresponding path loss factor.

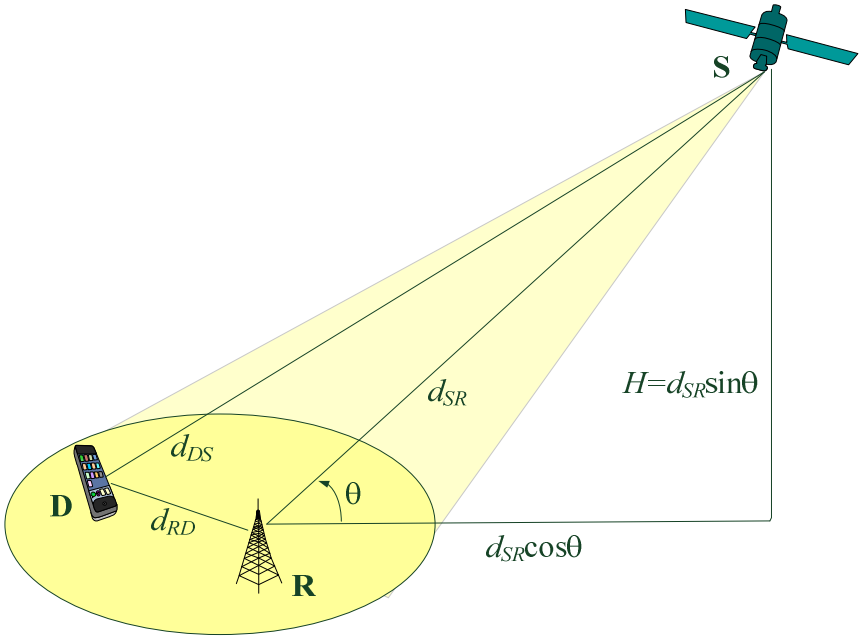

Figure 1. The system model

- The satellite-terrestrial link between the source S and the relay R, denoted as S-R, with the instantaneous SNR at the relay:

$$\gamma_2(t)=\frac{P_S}{\sigma^2 d_{SR}^{n_{SR}}}\left|h_2(t)\right|^2=\overline{\gamma}_2\left|h_2(t)\right|^2, \tag{2}$$

where h_2 denotes the channel gain between the source and the relay, d_{SR} denotes its distance, and n_{SR} is the corresponding path loss factor.

- The terrestrial link between the relay R and the destination D, denoted as R-D, with the instantaneous SNR at the relay:

$$\gamma_3(t)=\frac{P_R}{\sigma^2 d_{RD}^{n_{RD}}}\left|h_3(t)\right|^2=\overline{\gamma}_3\left|h_3(t)\right|^2, \tag{3}$$

where h_3 denotes the channel gain between the relay and the destination, d_{RD} denotes its distance, and n_{RD} is the corresponding path loss factor.

TABLE I

TYPICAL SIMULATION PARAMETERS [9]

Propagation scenario	b_0	m	Ω
Infrequent light shadowing	0.158	19.4	1.29
Average shadowing	0.126	10.1	0.835
Frequent heavy shadowing	0.063	0.739	0.000897

A. CHANNEL MODEL IN SATELLITE-TERRESTRIAL LINKS

The satellite-terrestrial channel is described by the shadowed Ricean fading model, where the complex channel gain $h(t)$ consists of the scattering component with the Rayleigh distributed envelope and line-of-sight (LOS) component with Nakagami-m distributed envelope.

The probability density function (PDF) of the power gain of the satellite-terrestrial channel with shadowed Ricean fading, denoted by $\lambda_i(t)=|h_i(t)|^2$, applicable for S-D and S-R links, is given by [5]

$$f_{\Lambda_i}(\lambda_i)=\left(\frac{2b_{0,i}m_i}{2b_{0,i}m_i+\Omega_i}\right)^m \frac{1}{2b_{0,i}} e^{-\frac{\lambda_i}{2b_{0,i}}} {}_1F_1\left(m_i;1;\frac{\Omega_i\lambda_i}{2b_{0,i}(2b_{0,i}m_i+\Omega_i)}\right),\ \lambda_i\geq 0,\ i=1,\ 2. \tag{4}$$

In the above expression, $2b_{0,i}$ denotes the average power of the scattering component, Ω_i is the average power of the LOS component, the Nakagami parameter for the LOS component is m_i, and ${}_1F_1(\cdot\,;\cdot\,;\cdot)$ is the confluent hypergeometric function of the first kind. The channel parameters that correspond to the typical propagation scenarios are presented in Table 1.

The above expression can be written in a more compact form if we apply the following substitutions

$$\alpha_i=\frac{1}{2b_{0,i}}\left(\frac{2b_{0,i}m_i}{2b_{0,i}m+\Omega_i}\right)^{m_i},\ \beta_i=\frac{1}{2b_{0,i}},\ \delta_i=\frac{\Omega_i}{2b_{0,i}(2b_{0,i}m_i+\Omega_i)}, \tag{5}$$

and in the special case of integer-valued parameters m_i, the hypergeometric function can be represented in the form of finite summation of polynomial-exponential terms by using Kummer's transform [4], resulting in PDF expression

$$f_{\Lambda_i}(\lambda_i)=\alpha_i\sum_{k=0}^{m-1}\varsigma_i(k)\lambda_i^k e^{-(\beta_i-\delta_i)\lambda_i},\ i=1,\ 2, \tag{6}$$

where $\varsigma_i(k)=(-1)^k(1-m_i)_k\,\delta_i^k/(k!)^2$, and $(t)_k=t(t+1)\cdots(t+k-1)$ denotes the Pochhammer symbol.

B. CHANNEL MODEL IN TERRESTRIAL LINKS

We assume that the envelope of the channel gain between R and D, denoted by $|h_3(t)|$, follows Nakagami distribution. Its squared value $\lambda_3(t)=|h_3(t)|^2$ is Gamma distributed

$$f_{\Lambda_3}(\lambda_3)=\frac{m_3^{m_3}\lambda_3^{m_3-1}}{\Omega^{m_3}\Gamma(m_3)}e^{-\frac{m_3\lambda_3}{\Omega_3}}, \tag{7}$$

where $\Omega_3=E\{\lambda_3\}$, m_3 denotes the fading parameter, and $\Gamma(.)$ denotes the Gamma function.

C. COOPERATIVE RELAYING TECHNIQUE

In the SR protocol, the following strategy of cooperative relaying is applied [1]:

- in the first half of the signalization interval, the receiver at the destination receives a signal from the source (link S-D is used for transmission, and the received SNR is γ_1);
- in the second half of the signalization interval, the receiver at the destination receives signal from the relay, only if the signal at the relay is correctly decoded (link R-D is used for transmission of signal with received SNR γ_3, only if the S-R link satisfies condition $\gamma_2 \geq \gamma_{th}$);
- the maximum ratio combining (MRC) is used at the receiver placed at the destination, i.e. the signals are combined (the corresponding SNRs are obtained as the addition of the SNRs in two intervals) [6]:

$$\gamma_{MRC} = \begin{cases} \gamma_1, & \gamma_2 < \gamma_{\text{th}}, \\ \gamma_1 + \gamma_3, & \gamma_2 \geq \gamma_{\text{th}}. \end{cases} \tag{8}$$

It can be noticed that the described protocol occupies two time slots, and the outage probability can be defined as [7]

$$P_{out} = \Pr\left(0.5\log_2(1+\gamma_{MRC}) \leq \log_2(1+\gamma_{\text{th,norm}})\right). \tag{9}$$

The above expression can be rewritten as

$$P_{out} = \Pr\left(\gamma_{MRC} \leq \gamma_{\text{th,norm}}^2 + 2\gamma_{\text{th,norm}}\right), \tag{10}$$

and we can define the threshold of the SNR at the output of MRC combiner as $\gamma_{\text{th}} = \gamma_{\text{th,norm}}^2 + 2\gamma_{\text{th,norm}}$ [7].

Using the above description of the cooperative relaying protocol, the outage probability of the system can be determined as [3]

$$P_{out}(\gamma_{\text{th,norm}}) = = \Pr\left(\gamma_{MRC} \leq \gamma_{\text{th}}\right) = \Pr(\gamma_2 < \gamma_{\text{th}})\Pr(\gamma_1 < \gamma_{\text{th}}) + \Pr(\gamma_2 \geq \gamma_{\text{th}})\Pr(\gamma_1 + \gamma_3 < \gamma_{\text{th}}). \tag{11}$$

2.2. OUTAGE PROBABILITY AND NUMERICAL RESULTS

The outage probability expression can be determined by using the PDFs of the SNR at the corresponding receivers [3]

$$P_{out} = \int_0^{\gamma_{\text{th}}} f_{\Gamma_2}(\gamma_2)d\gamma_2 \int_0^{\gamma_{\text{th}}} f_{\Gamma_1}(\gamma_1)d\gamma_1 + \int_{\gamma_{\text{th}}}^{\infty} f_{\Gamma_2}(\gamma_2)d\gamma_2 \int_0^{\gamma_{\text{th}}} f_{\Gamma_1}(\gamma_1) \int_0^{\gamma_{\text{th}}-\gamma_1} f_{\Gamma_3}(\gamma_3)d\gamma_3 \, d\gamma_1. \tag{12}$$

The first and the second integral in the above expression corresponds to the cumulative distribution function (CDF), that is given with expression [4]

$$I_i = \int_0^{\gamma_{\text{th}}} f_{\Gamma_i}(\gamma_i)d\gamma_i = F_{\Gamma_i}(\gamma_{th}) = 1 - \alpha_i \sum_{k=0}^{m_i-1} \frac{\varsigma_i(k)}{\overline{\gamma}_i^{k+1}} \sum_{p=0}^{k} \frac{k!}{p!} \left(\frac{\beta-\delta}{\overline{\gamma}_i}\right)^{-(k+1-p)} \gamma_{th}^p \, e^{-\frac{\beta-\delta}{\overline{\gamma}_i}\gamma_{th}}, \; i = 1,2. \tag{15}$$

By using the previous expression, the third integral is also easily obtained as

$$I_3 = \int_{\gamma_{th}}^{\infty} f_{\Gamma_2}(\gamma_2) d\gamma_i = 1 - F_{\Gamma_2}(\gamma_{th}) = \alpha_2 \sum_{k=0}^{m_2-1} \frac{\varsigma_2(k)}{\bar{\gamma}_2^{k+1}} \sum_{p=0}^{k} \frac{k!}{p!} \left(\frac{\beta - \delta}{\bar{\gamma}_2} \right)^{-(k+1-p)} \gamma_{th}^{p} e^{-\frac{\beta-\delta}{\bar{\gamma}_i}\gamma_{th}}. \quad (16)$$

Finally, as we shown in [8], the double integral can be simplified if we notice that the inner integral can be represented as the CDF of random variable γ_3, for the argument γ_{th}-γ_1, to obtain

$$I_4 = \int_0^{\gamma_{th}} f_{\Gamma_1}(\gamma_1) F_{\Gamma_3}(\gamma_{th} - \gamma_1) d\gamma_1 = \int_0^{\gamma_{th}} f_{\Gamma_1}(\gamma_1) \left(1 - \frac{\Gamma\left(m_3, \frac{m_3}{\Omega_3 \bar{\gamma}_3}(\gamma_{th} - \gamma_1) \right)}{\Gamma(m_3)} \right) d\gamma_1. \quad (17)$$

where $\Gamma(.,.)$ denotes the upper incomplete Gamma function [9]. To the best of our knowledge, only the numerical solution of the above integral, for the special case when $\bar{\gamma}_3 = 1$, was considered in the paper [7]. If we introduce the substitutions

$$A_k = \frac{\varsigma_1(k)}{\bar{\gamma}_1^{k+1}},\ B = \frac{\beta_1 - \delta_1}{\bar{\gamma}_1},\ C = \frac{m_3}{\Omega_3 \bar{\gamma}_3}, \quad (21)$$

by using simple mathematical operations, described in [8], we obtain the following closed-form solution of the double integral from Eq. (12):

$$I_4 = \alpha_1 \sum_{k=0}^{m_1-1} A_k \left[\frac{k!}{B^{k+1}} - e^{-B\gamma_{th}} \sum_{j=0}^{k} \frac{k!}{j!} \frac{\gamma_{th}^j}{B^{k-j+1}} \right] + \alpha_1 \sum_{k=0}^{m_1-1} \sum_{p=0}^{m_3-1} \sum_{q=0}^{p} \binom{p}{q} \frac{(-1)^q A_k C^p}{p!} \gamma_{th}^{p-q} e^{-C\gamma_{th}}$$
$$\times \left[\frac{(k+q)!}{(B-C)^{k+q+1}} - e^{-(B-C)\gamma_{th}} \sum_{j=0}^{k+q} \frac{(k+q)!}{j!} \frac{\gamma_{th}^j}{(B-C)^{k+q-j+1}} \right]. \quad (22)$$

Numerical results will be presented for a LEO system, with the following typical parameters for the satellite-terrestrial part of the system: H = 550 km, L = 25 km, P_S = 25 dBW, σ^2 = -64 dBm, and path-loss factor $n_{SD} = n_{SR} = 2$. We assume that the elevation angles at the destination and relay satisfy condition $\theta_R \approx \theta_D = \theta$, and the corresponding distances from the satellite are approximately the same, i.e. $d_{SD} \approx d_{SR} = H/\sin(\theta)$, and $\bar{\gamma}_1 = \bar{\gamma}_2$. In the satellite-terrestrial link, we assume carrier frequency f_0 = 11 GHz, typical for Ku-band and downlink channels. On the other hand, in R-D terrestrial link we assume f_0 = 4 GHz, typical for microwave communications.

By using the algorithm described in our recent work [10], we have generated the correlated time series that corresponds to the complex channel gains in two satellite-terrestrial links, i.e. $h_1(t)$ and $h_2(t)$. We assumed the isotropic scattering with the normalized autocorrelation function $R_r(\tau) = J_0(2\pi f_{Dm}\tau)$, where f_{Dm} denotes the maximum Doppler shift. In our simulations, we assume f_{Dm} = 100 Hz. As the shadowing typically varies much slower, we chose f_{Ds} = 1Hz [11].

The same simulator, with slight modification, can be used to generate temporally correlated complex gain $h_3(t)$ for terrestrial link R-D. The propagation is also isotropic, with f_{Dm} = 18.5 Hz (corresponds to v = 5 km/h, for reduced carrier frequency when compared with links S-D and S-R). In the terrestrial network and urban environment, we apply the path-loss factor n_{RD} = 4 [12], the noise power is σ^2 = -64 dBm. The waveforms for the received SNRs at the receivers are obtained sample-by-sample by using Eqs. (1) - (3). The outage probability is estimated on basis of $N = 10^8$ samples.

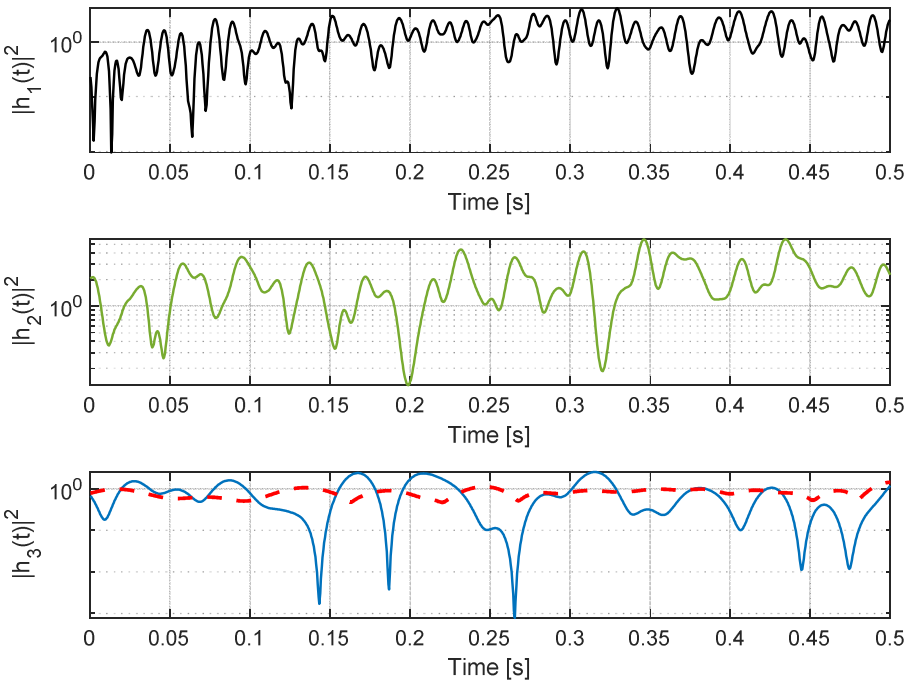

Fig. 2. Instantaneous power gains for S-D, S-R, and R-D links.

The instantaneous power gains, obtained from the channel coefficients are shown in Fig. 2. The waveforms are presented for a case when there is an average shadowing at the S-D link, and there is a light shadowing at the S-R link (the relay is usually placed at a location where LOS component is strong).

The values from Table 1 are used for satellite-terrestrial links, where the fading parameter is rounded to the nearest integer, i.e. m_1 = 10, m_2 = 19. For the terrestrial link R-D we chose parameter Ω_3=0.835, and we consider the propagation without LOS component (m_3 = 1) and with strong LOS component (m_3 = 20).

First, we will analyze the simplified scenario, where $\overline{\gamma}_i = 1,\ i = 1,2,3.$ In such a case, our analysis corresponds with the numerical results presented in [3]. The resulting outage probability is presented in Fig. 3. It is obvious that the increase of parameter m_3 has a positive impact as it decreases the outage probability.

A more realistic scenario is based on assumption that a typical value of the elevation angle is equal to θ_{ref} = 60°, and we set a referent distance between R and D to $d_{RD,ref}$ = 10 km (the numerical value depends on the beam diameter). In such a case, $d_{SDref}=H/\sin(\theta_{ref})$ denotes the referent distance between S and D, and the transmitted power at the relay can be adjusted to satisfy the equation

$$P_R = P_S \times d_{RD,ref}^{n_{RD}} / d_{SD,ref}^{n_{SR}}. \tag{23}$$

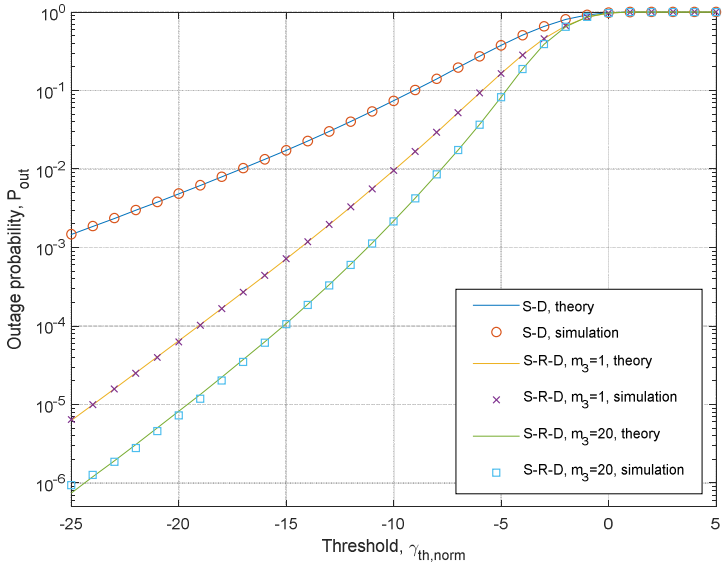

Fig. 3. Outage probability for the case of equal average received powers at the destination receiver – average shadowing at S-D link; light shadowing at S-R link; terrestrial link with Ω_{RD}=0.835, fading parameters m_3=1 and m_3=20.

It can be noticed from Fig. 2 that higher m_3 corresponds to a more stable signal at the R-D link. A similar effect can be noticed in Fig. 4, where the system geometry is taken into account and the instantaneous SNR at the MRC output is presented. As the receiver is mobile, the distance d_{RD} is not fixed and the received SNR at the R-D link can vary a lot for the fixed power P_R, calculated according to Eq. (23). If $\theta = 60^o$ and d_{RD} = 10 km, the average SNRs at the receivers are same, $\overline{\gamma}_1 = \overline{\gamma}_2 = \overline{\gamma}_3$. If $\gamma_2 \leq \gamma_{th}$, the output SNR at the MRC combiner is $\gamma_{MRC} = \gamma_1$, while for $\gamma_2 > \gamma_{th}$, the output SNR is $\gamma_{MRC} = \gamma_1 + \gamma_3$. The P_{out} for γ_{MRC} will be reduced if $\overline{\gamma}_3 > \overline{\gamma}_1$ and/or if γ_3 has not significant fluctuation.

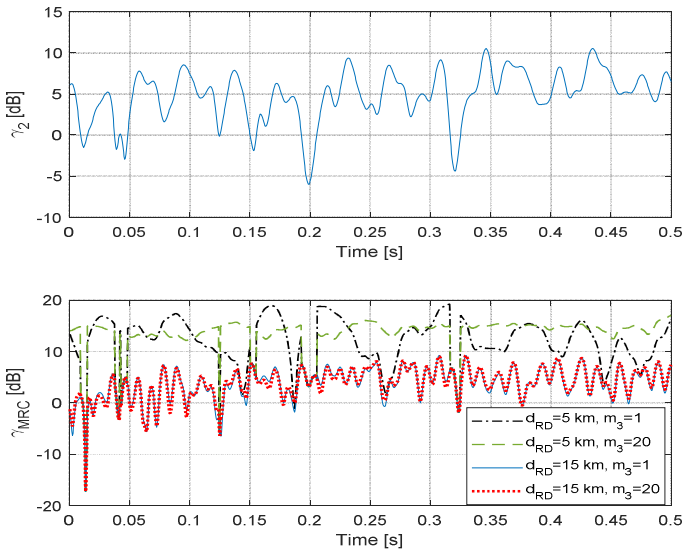

Fig. 4. The waveforms of the instantaneous SNRs at the S-R link and at the output of the MRC receiver at the destination.

In Figure 5, we present the effect of variable distance d_{RD} when m_3 = 1 and m_3 = 10, for the fixed value Ω_3 = 0.835, and the parameters for S-D and S-R link are same as in Figs. 2 and 3 (average shadowing at S-D link, light shadowing at the S-R link, and $\overline{\gamma}_1 = 2.95$ dB). The outage probability is reduced for d_{RD} = 5 km (where $\overline{\gamma}_3 = 14.98 \text{ dB} > \overline{\gamma}_1$), as the effect of the relay presence is more significant when compared to the case when d_{RD} = 15 km (where $\overline{\gamma}_3 = -4.1 \text{ dB} < \overline{\gamma}_1$).

As expected, the outage probability is lower for larger values of fading parameter m_3, as the signal at the R-D link is more stable in this case. It is interesting that the effect of higher m_3 is minor for large thresholds, especially for larger distances d_{RD}, as the outage probability for m_3=10 has approximately the same value as in the case when m_3=1. In such a case, relay does not improve significantly the overall system performance. On the contrary, for small values of the SNR thresholds, for large values of m_3 we obtain approximately the same value of P_{out} for the cases when d_{RD} = 15 km, d_{RD} = 10 km, and d_{RD} = 5 km. This effect can be easily explained if we observe Fig. 4 – large values of m_3 correspond to fewer fluctuations in γ_3, and in the case when $\gamma_2 \le \gamma_{th}$, the output of the MRC combiner $\gamma_{MRC} = \gamma_1 + \gamma_3$ is on a high level, with a minor probability of outage. In such a case, most outages happen when $\gamma_2 \le \gamma_{th}$, and the corresponding probability does not depend on the distance d_{RD}, which does characterize R-D link.

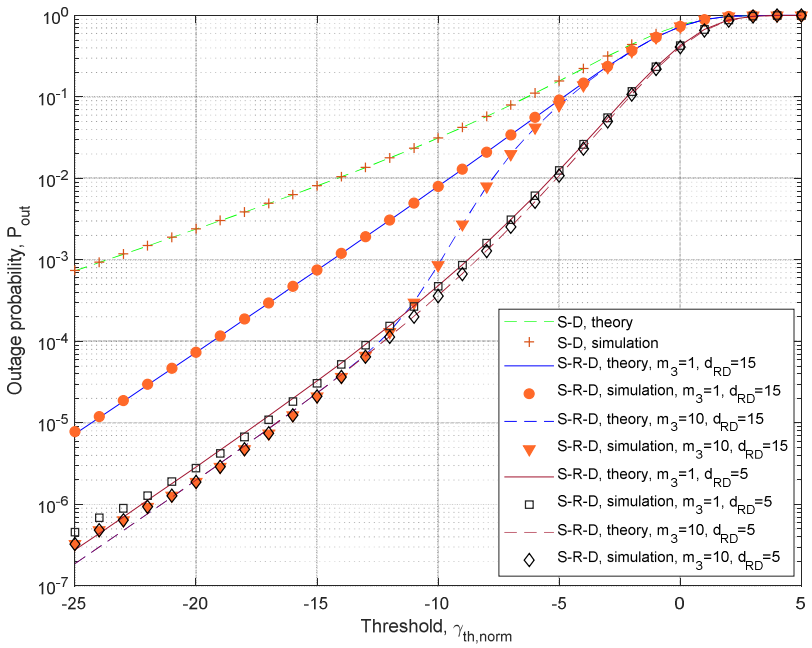

Fig. 5. Outage probability for different distances between R and D, for the typical value of the elevation angle.

In Figure 6, we present the numerical results for various elevation angles. In this scenario, the referent value for R-D distance is fixed to d_{RD} = 10 km, which corresponds to $\overline{\gamma}_3 = 2.95$ dB. Although the mobile user does not change its position, the LEO satellites have high velocity and their elevation angle can change significantly in a few minutes. The numerical results are presented for three characteristic elevation angles: θ = 40°, θ = 60°, and θ = 80°. The other system parameters are fixed as in the previous simulations.

For the lower elevation angles, the average SNR is reduced both at satellite-terrestrial links (S-D and S-R). As the instantaneous SNR is also reduced, the average P_{out} increases for lower □. Although the elevation angle does not impact the terrestrial link R-D, it cannot dramatically improve the overall system performance if $\overline{\gamma}_3 \approx \overline{\gamma}_1$. In this case, the outage probability is dictated by the reduced performance of the S-R link. On the other hand, for higher values of m_3 or $\overline{\gamma}_3$, the outage performance are improved (the combination of the effects from Fig. 5 and Fig. 6). Therefore, the tunable transmit power of the relay should potentially compensate this effect of the degraded system performance due to the reduced elevation angle.

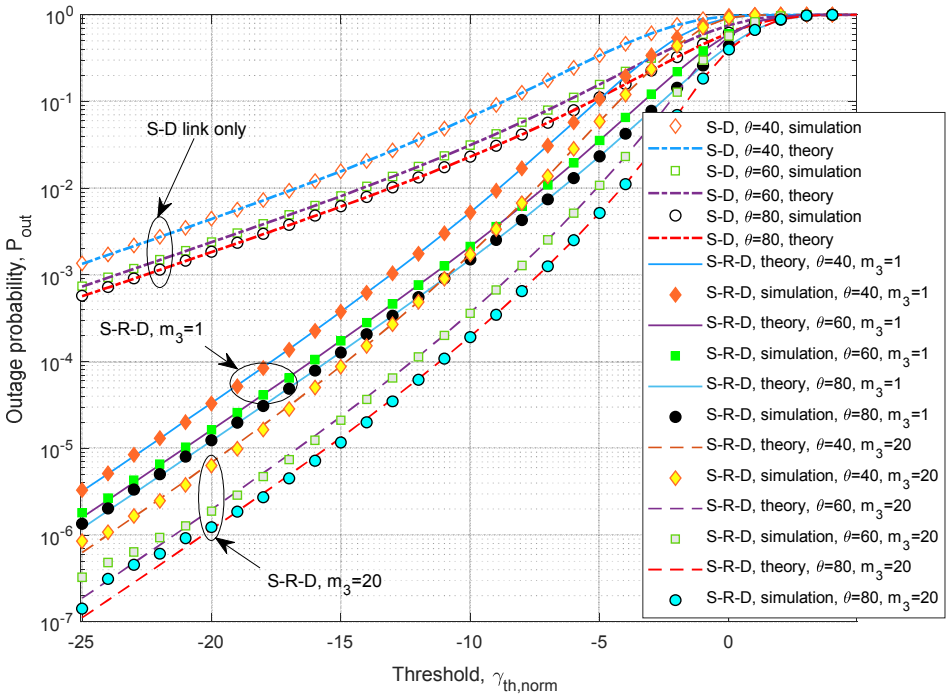

Fig. 6. Outage probability for different distances between S and D, S and R, for the typical value of the distance between R and D.

SECTION 3 – ENERGY EFFICIENT TERRESTRIAL SYSTEMS FOR INTERNET OF THINGS APPLICATIONS

As the number of devices and services in the field of wireless communications has been constantly growing, the introduction of new concepts capable of meeting the set of demands with available resources becomes a necessity. In addition to provision of higher bandwidth, better coverage, and reliable connections, 5G and beyond 5G technologies are expected to provide considerable energy savings and extremely low latency for various classes of users. 5G networks also represent an essential component in the development of the IoT (Internet of Things) systems, that assume connection of a high number of devices, sensors, objects and applications to the Internet. These applications will be able to collect huge amounts of data from various devices and sensors, and can be encountered in a wide range of applications (commercial, health, security applications, as well as the industrial ones, known as the Industrial Internet of Things). The increasing challenges concerning the provision of 5G services and applications in various environments might be solved through the integration of satellite, aerial and terrestrial systems. As the integrated systems are intended for the improved support of diverse IoT applications, the spectrum and energy efficiency of all subsystems has also attracted a lot of attention, recently. The following activities are related to the analysis of the spectral efficiency of the energy efficient terrestrial part of the network with and without additional aerial network component support. The usage of aerial component is very important as the implementation of wireless sensor network (WSN) can be required in remote and hardly accessible or toxic areas in an uninhabited or industrial environment, where it is challenging to provide a reliable data collection system. Moreover, in areas that are under risk of natural disasters, special attention should be placed on data collection system design in the case when conventional power and communication infrastructure is destroyed. The usage of unmanned aerial vehicles (UAVs) can be very useful in variable environments, as it offers numerous advantages such as the possibility of providing mobile data collectors that can be used in special monitored areas, that are not easily approachable or not convenient for ground-based data collectors. Moreover, if a sensor network is deployed over a large area, the aerial components can contribute to faster search and lower energy consumption of sensor nodes as UAVs can enable data collection with shorter propagation paths between the transmitter and the receiver, thus reducing path losses. Therefore, the employment of UAV for data collection leads to lower latency, as well as higher reliability and quality of service (QoS).

Furthermore, in numerous scenarios, the WSN must be set in an environment where the infrastructure is hardly available. In that case, it is essential to provide a robust energy power supply, as the positions of the sensor network nodes might be inaccessible, and the reliance on frequent battery replacement is impractical. Various existing natural energy sources could be used for enabling energy needed for the communication purposes, since the sensor nodes has limited power resources. The main disadvantage is that these sources are not reliable as they depend on unpredictable circumstances such as weather conditions, etc. Simultaneous information and power transfer (SWIPT) represents an appealing technology for various applications within contemporary communication systems, with the main advantage resulting from the capability of using RF signals for carrying both energy and information. One of the possible feasible approaches for WSN powering is also the use of the dedicated, power beacon (PB) node.

3.1. APPLICATIONS OF AERIAL COMPONENTS IN TERRESTRIAL PART OF THE NETWORK

In this activity we present the performance analysis of the WSN with the ground-based PB node [13]. The UAV is utilized for data collection in an energy-constrained WSN. The analyzed scenario is important for industrial applications in the cases where the ground-based power supply PB node can be enabled, but due to lack of the telecommunication infrastructure in the area, the ground-based data collecting system represents an issue. This subsystem can easily be integrated with the satellite part of the system, thus forming reliable telecommunication infrastructure in remote areas or disaster-affected areas.

Therefore, we analyze a PB-assisted WSN where data collecting is realized with the help of the UAV. The system performances are analyzed under the general assumption that the fading in the propagation environment is subject to Nakagami-*m* distribution, since this distribution encompasses various channel fading scenarios as special cases. It is further assumed that power transfer from the PB to the IoT sensor and further information transfer to the UAV data collector is performed according to the time-switching (TS) protocol, which means that in the each time frame part of the time is dedicated for power transfer, while the rest of the time frame is used for the information transfer [13]. We assume that the IoT sensor node is in active transmission mode and sends information to the UAV, which is uniformly randomly positioned within a circle of a certain radius *R* at a given height *H*.

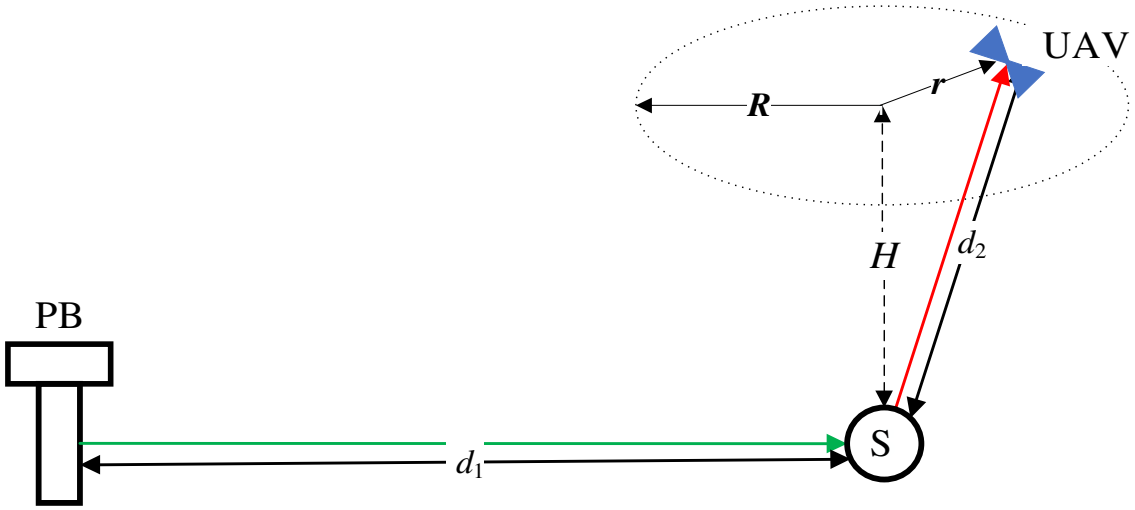

Figure 7. IoT system model with UAV based data collector.

The model of the considered system is presented in Figure 7. It is composed of an energy limited IoT sensor (S) and a power beacon that is used for sensor node power supply. As the sensor network is positioned in an inaccessible area, a UAV is used to collect the information from the sensor node. It is assumed that during the collecting time interval, the UAV is positioned at a height H and its position is random within a flying area - a circle of radius R above the sensor node.

The fading envelopes in the channels from the PB to the source and from the source to the UAV are denoted by h_1 and h_2, while the corresponding distances between the nodes are equal d_1 and d_2, respectively. The path loss coefficients in the channels from the PB to the source and from the source to the UAV are denoted by are δ_1 and δ_2, respectively. The fading envelopes are modelled by the Nakagami-m distribution with mean values $\overline{\gamma}_i = \mathrm{E}\{\gamma_i\}$ and fading parameters m_i, i = 1, 2.

The sensor harvests the RF energy transmitted from the PB in accordance with the TS protocol and further uses the accumulated energy to transmit information to the UAV. According to the protocol, within the transmission block time of duration T, the sensor harvests the RF energy from the PB during the first part αT, $0 \le \alpha < 1$, while the remaining time duration equal $(1-\alpha)T$ is used to transmit signals to the UAV. The transmit power of the beacon is equal P_B, while η ($0 < \eta < 1$) denotes the efficiency of the energy conversion.

In order to collect the information from the sensor, the UAV is located within a flying area, which represents a circle with radius R at the height H above the sensor node. The origin of the circle is centered directly above the sensor and the UAV distance from the circle origin equal r is uniformly distributed according to the following PDF [14]

$$p_r(r) = \frac{2}{R^2} r\,.$$

As the distance between the sensor and the UAV can be expressed as $d_2 = \sqrt{H^2 + r^2}$, it has been shown that the outage probability of the system can be expressed as

$$P_{out}(\gamma_{th}) = \frac{2\gamma_{th}^{\frac{m_1+m_2}{2}}}{\Gamma(m_1)\Gamma(m_2)\delta_2 R^2}\left(\frac{(1-\alpha)m_1 m_2 d_1^{\delta_1}\sigma^2}{\overline{\gamma}_1\overline{\gamma}_2\eta\alpha P_B}\right)^{\frac{m_1+m_2}{2}}\left(\left(H^2+R^2\right)^{\frac{\delta_2}{2}\left(\frac{m_1+m_2}{2}+\frac{2}{\delta_2}\right)}\right.$$

$$\times G_{2,4}^{2,2}\left(\frac{(1-\alpha)m_1 m_2 d_1^{\delta_1}\sigma^2\gamma_{th}\left(H^2+R^2\right)^{\frac{\delta_2}{2}}}{\overline{\gamma}_1\overline{\gamma}_2\eta\alpha P_B}\middle|\begin{matrix}1-\frac{m_1+m_2}{2}, 1-\frac{m_1+m_2}{2}-\frac{2}{\delta_2}\\ \frac{m_2-m_1}{2}, \frac{m_1-m_2}{2}, -\frac{m_1+m_2}{2}-\frac{2}{\delta_2}, -\frac{m_1+m_2}{2}\end{matrix}\right)$$

$$\left.-H^{\delta_2\left(\frac{m_1+m_2}{2}+\frac{2}{\delta_2}\right)} G_{2,4}^{2,2}\left(\frac{(1-\alpha)m_1 m_2 d_1^{\delta_1}\sigma^2\gamma_{th}H^{\delta_2}}{\overline{\gamma}_1\overline{\gamma}_2\eta\alpha P_B}\middle|\begin{matrix}1-\frac{m_1+m_2}{2}, 1-\frac{m_1+m_2}{2}-\frac{2}{\delta_2}\\ \frac{m_2-m_1}{2}, \frac{m_1-m_2}{2}, -\frac{m_1+m_2}{2}-\frac{2}{\delta_2}, -\frac{m_1+m_2}{2}\end{matrix}\right)\right).$$

Further, the outage capacity is given by the following expression

$$C_{out} = \frac{1}{\ln 2}\left(1 - P_{out}(\gamma_{th})\right)\ln\left(1+\gamma_{th}\right),$$

while the corresponding throughput is given by

$$T_{out} = (1-\alpha)C_{out}\,.$$

By applying the statistical averaging, the ergodic capacity of the considered system can be expressed in the following exact closed-form

$$C_{erg}=\frac{1}{\ln 2}\frac{2}{\Gamma(m_1)\Gamma(m_2)}\frac{1}{\delta_2 R^2}\left(\frac{(1-\alpha)m_1m_2d_1^{\delta_1}\sigma^2}{\overline{\gamma}_1\overline{\gamma}_2\eta\alpha P_B}\right)^{\frac{m_1+m_2}{2}}$$

$$\times\left(\left(H^2+R^2\right)^{\frac{\delta_2}{2}\left(\frac{m_1+m_2}{2}+\frac{2}{\delta_2}\right)}\int_0^{\infty}x^{\frac{m_1+m_2}{2}-1}G_{1,3}^{2,1}\left(\frac{(1-\alpha)m_1m_2d_1^{\delta_1}\sigma^2x}{\overline{\gamma}_1\overline{\gamma}_2\eta\alpha P_B}\left(H^2+R^2\right)^{\frac{\delta_2}{2}}\middle|\begin{matrix}1-\frac{m_1+m_2}{2}-\frac{2}{\delta_2}\\ \frac{m_2-m_1}{2},\frac{m_1-m_2}{2},-\frac{m_1+m_2}{2}-\frac{2}{\delta_2}\end{matrix}\right)G_{2,2}^{1,2}\left(x\middle|\begin{matrix}1,1\\1,0\end{matrix}\right)\mathrm{d}x\right.$$

$$\left.-H^{\delta_2\left(\frac{m_1+m_2}{2}+\frac{2}{\delta_2}\right)}\int_0^{\infty}x^{\frac{m_1+m_2}{2}-1}G_{1,3}^{2,1}\left(\frac{(1-\alpha)m_1m_2d_1^{\delta_1}\sigma^2x}{\overline{\gamma}_1\overline{\gamma}_2\eta\alpha P_B}H^{\delta_2}\middle|\begin{matrix}1-\frac{m_1+m_2}{2}-\frac{2}{\delta_2}\\ \frac{m_2-m_1}{2},\frac{m_1-m_2}{2},-\frac{m_1+m_2}{2}-\frac{2}{\delta_2}\end{matrix}\right)G_{2,2}^{1,2}\left(x\middle|\begin{matrix}1,1\\1,0\end{matrix}\right)\mathrm{d}x\right),$$

while the corresponding throughput is given by

$$T_{erg}=(1-\alpha)C_{erg}.$$

The correctness of derived expressions is confirmed by using independent Monte Carlo simulation method. The provided analysis and the obtained numerical results can be used as a guidance for the design of UAV data collection system in inaccessible area. For example, described system model corresponds to the scenario where access to IoT sensors in the industrial zones is difficult, and the UAV provides the collection of information from the sensors. Furthermore, the considered system model and given performance analysis can be used in natural disaster scenarios (such as floods or earthquakes), when the UAV is randomly distributed in the circular disaster area and has a roll of data-collection stations. Based on the obtained analytical and simulation results we demonstrate the characteristics of the network for various system parameters and propagation conditions including the randomness of the UAV locations.

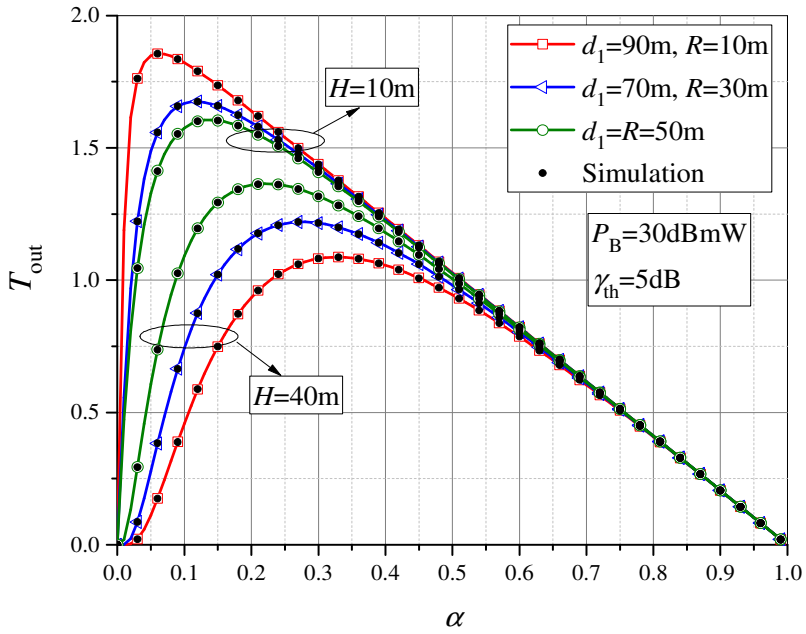

Figure 8. The outage throughput dependence on the TS coefficient α, for various values of height *H*.

The throughput T_{out} is shown in Figure 8 in the function of the time-switching parameter α. Results are presented for various values of UAV altitude and various ratios of distance d_1 and radius R. For higher values of altitude H, when the sensor is closer to PB, it takes less time to charge the sensor, i.e., the maximum value of T_{out} is obtained for a smaller optimal value of time-switching coefficient. At lower altitudes (H = 10 m), throughput is higher due to the smaller distance d_2, the sensor needs less energy to send information, so the optimal value of time-switching coefficient is smaller. Moreover, it can be seen in this case that a smaller value of R leads to larger value of throughput T_{out}.

Within this activity, the application of aerial network component is also analyzed for an industrial-service communication system, illustrated in Figure 9. The considered system represents a possible solution for the natural disaster scenarios [15]. In this case, the aerial, UAV component of the system serves both as information relay as well as the power supply node for the energy-limited node. The traditional communication infrastructure can be disrupted or even completely unavailable due to natural or human disasters (such as earthquakes, floods, bushfires, and tornadoes), demanding the employment of emergency wireless networks. We consider a general system model that can be applied as a SCADA system, which consists of an master terminal unit (MTU), an remote terminal unit (RTU), and an end user terminal (UT), where the RTUs are used at remote destinations and are usually placed in outdoor inaccessible environments. SCADA architecture is utilized for monitoring and management of industrial processes. Therefore, the MTU can send information to the RTU to provide an emergency shutdown of the process, to prevent hazardous situations by starting or stopping pumps or adjusting the speed of pumps, and to regulate the flow of fluids or gases by opening/closing valves. The industrial control functions are performed by using the communication link, which consists of the MTU-RTU and the RTU-UT hops, but according to the predicted scenario, the communication between the master and the remote unit is disrupted. In addition, the RTU is an energy-limited device left without conventional power supply due to disaster conditions. In such a scenario, the UAV is employed as a relay for information transfer between the MTU and the RTU. It also serves as an energy supplier for the RTU, thus enabling data transmission from the MTU to the end user.

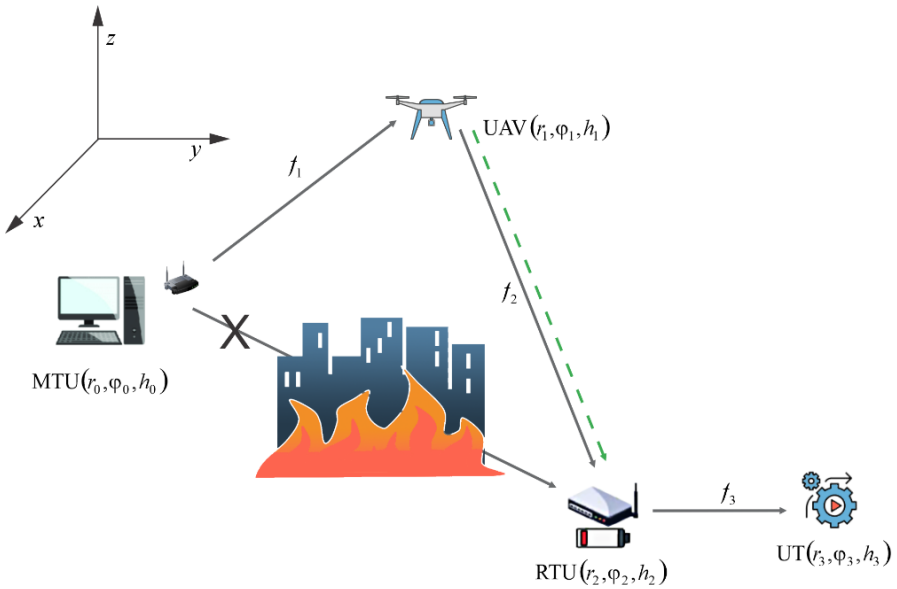

Figure 9. UAV-assisted industrial system for emergency applications.

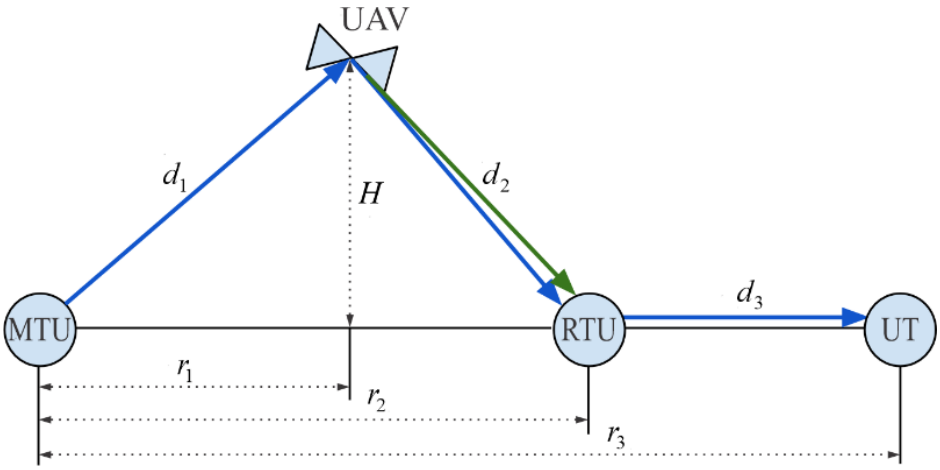

Figure 10. Nodes' positions in UAV-assisted industrial system for emergency applications.

The novel outage probability and throughput expressions are derived for the considered multihop Nakagami-*m*/Nakagami-*m*/Fisher–Snedecor relaying system, with a UAV employed as a DF relay and energy supplier for RTU. The outage performance and end-to-end system throughput analysis is provided, with an aim to adjust the UAV's relative position above the MTU-RTU link and the amount of supplied power in relation to other essential parameters. The Monte Carlo simulation model of the system is developed to confirm the correctness of the derived expressions. Numerical results based on both analytical expressions and simulation results are provided.

The location of each network node is determined in the cylindrical coordinate system as MTU(r_0, φ_0, h_0), UAV(r_1, φ_1, h_1), RTU(r_2, φ_2, h_2), and UT(r_3, φ_3, h_3). For the sake of simplicity, the coordinates of the nodes' positions, for the presented numerical results, are MTU(0 m, 0 rad, 0 m), UAV(r_1, 0 rad, H), RTU(400 m, 0 rad, 0 m), and UT(450 m, 0 rad, 0 m). Consequently, the system model can be redrawn as in Figure 10. The distances between nodes d_i, i = 1, 2, 3, are defined by the Euclidean norm. Further, the following system parameters are set as ϑ = 0.8, δ_1 = δ_2 = δ_3 = 2.05, $\sigma_1^2 = 10^{-5}\text{mW}$, and $\sigma_2^2 = \sigma_3^2 = 10^{-7}\text{mW}$. In addition, the fading parameters that describe conditions of channels are set as m_1 = 5 for the MTU-UAV link, m_2 = 2 for the UAV-RTU link, and m_3 = 3.5 and m_{s3} = 5 for the RTU-UT link.

According to Figure 11, the specified distances in the MTU-UAV, the UAV-RTU, and the RTU-UT links are $d_1 = \sqrt{r_1^2 + H^2}$, $d_2 = \sqrt{(r_2 - r_1)^2 + H^2}$, and $d_3 = |r_3 - r_2| = 50\text{m}$, respectively. The dependence of the outage probability on the horizontal MTU-UAV distance is presented in Figure11, for various values of P_S. When the UAV is located closer to the MTU (r_1 < 200 m), the impact of the transmitted MTU power on the outage probability is negligible and by increasing the distance r_1, the outage probability decreases. For the certain horizontal MTU-UAV distance value, the minimum probability of outage occurs. The outage probability increases with the further increase in distance r_1. This effect can be intuitively explained by the fact that if the wireless power transfer is applied for the RTU power supply, the best performance is obtained when the UAV is directly above the RTU. However, this fact is valid only for higher values of P_S;

thus, the outage of the MTU-UAV link does not affect the overall outage performance. In general, the optimal location of the UAV that contributes to the minimum of the outage probability is located between the MTU and the RTU. For smaller values of P_S, the optimal performance is obtained when the UAV is positioned closer to the MTU, and vice versa. The best outage performance is obtained in the case of high MTU output power, when the UAV is positioned directly above the RTU, which harvests the energy from the UAV.

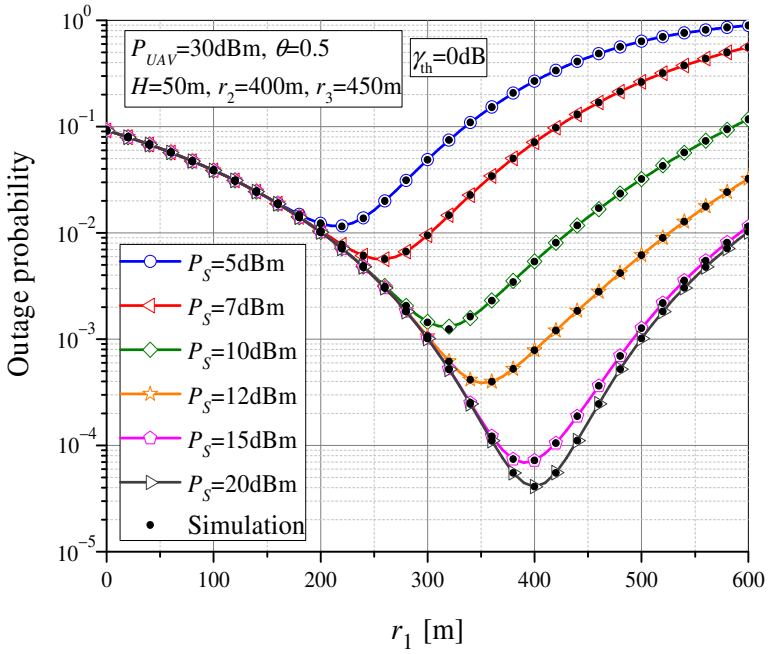

Figure 11. The outage probability vs. MTU-UAV horizontal distance for various values of MTU output power.

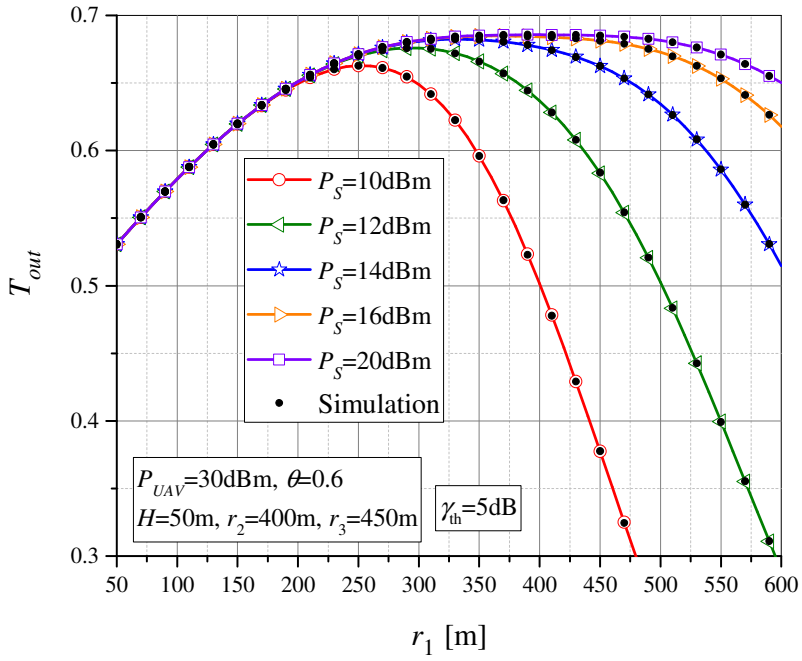

Figure 12. The throughput vs. MTU-UAV horizontal distance for various values of MTU output power.

In Figure 12, the throughput T_{out} is shown as a function of MTU-UAV horizontal distance, r_1, for various system parameter values and γ_{th} = 5 dB. The results are presented for different values of MTU output power, P_S. It can be noticed that for each value of P_S, there is an optimal UAV position at which maximum throughput T_{out} is achieved. When the UAV is closer to the MTU, the transmitted MTU power does not affect the throughput and it is determined by the UAV-RTU-UT subsystem. However, as the UAV-MTU distance increases, the throughput also increases due to smaller UAV-RTU distance. At a certain distance r_1, the maximum throughput can be reached. With the increase in MTU transmit power P_S, the value of maximum throughput also increases, and it is achieved for higher values of distance r_1. With a further increase in r_1 (beyond the one that maximizes throughput), the throughput decreases, and the overall system performance worsens.

3.2. THE ANALYSIS OF THE TERRESTRIAL PART OF THE NETWORK WITH MOBILE END-USER

This activity encompasses the application of wireless PB powering in the terrestrial part of the network and analysis of spectrally efficient scenario, where the considered terrestrial system is cognitive and shares the spectrum with the primary user, based on underlay concept [16].

Due to enormous number of low-power devices in IoT concept, the task of massive data transfer becomes an issue and creates the need for additional spectrum resources, more efficient spectrum access and innovative approaches. As the majority of spectrum is already allocated according to the current allocation policy, the usage of novel techniques for efficient spectrum usage is obligatory. Cognitive radio represents an innovative concept with the potential to solve the problem of spectrum scarcity [17] and has already been recognized in the literature as an important promising approach for IoT applications [18]. Two types of users can be distinguished in the concept of cognitive radio, the primary (licensed users) and secondary users that are allowed to simultaneously use the resources under the predefined rules [17]. In the underlay concept, the simultaneous communication of SUs with PUs is enabled, provided that harmful interference to the PUs is prevented by using the SU's transmit power adaptation. If the perfect channel state information (CSI) is available, the level of interference occurring at the PU receiver can vary within a certain tolerable limits. However, the realistic dynamic environment is characterized by constantly changing conditions, resulting practically in erroneous or outdated CSI, even in the concepts where the necessary feedback in the system exists [19]. As IoT nodes are usually low-power and computationally limited, the approach based on statistical CSI can be beneficial for energy efficiency, as it simplifies extensive calculations needed for power adaptation in conventional cognitive underlay concept.

In addition, the novel system generation is characterized by high user mobility, which significantly affects the performance of the wireless system due to the variability of the reception power [20]. We have described the user's movement using the random waypoint (RWP) model, that can describe the user's movement through three different patterns, depending on whether the user is moving through 1D, 2D or 3D systems [21].

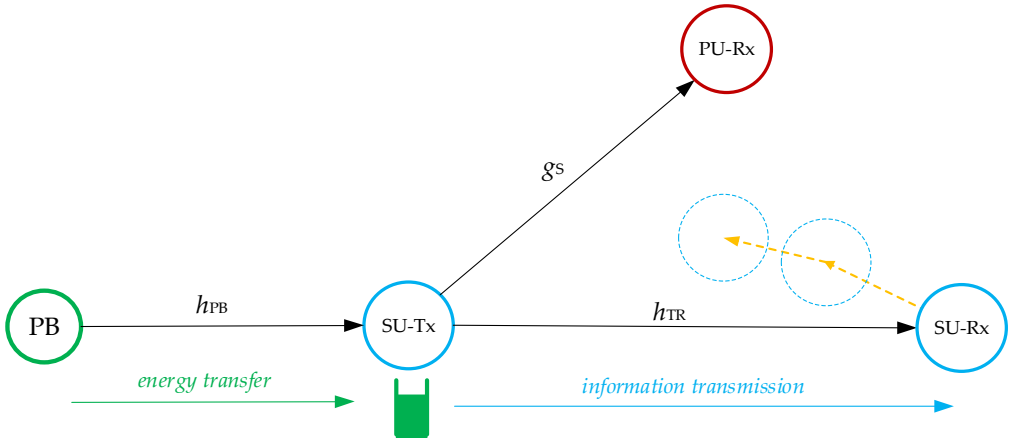

Figure 13. Model of the power beacon assisted underlay cognitive network with random mobility user.

In this activity the performance analysis of a cognitive wireless system with a mobile receiver was provided for the case of Nakagami-*m* fading environment. This work is motivated by the fact that there is a growing number of connected IoT devices, unsolved issues concerning their supply, as well as the increasing need for efficient solutions for spectrum access. We analyze a system where the transmitter is wirelessly powered using PB, while efficient spectrum access and information transfer are enabled by simultaneous spectrum usage with the primary users without jeopardizing conditions imposed by the primary network. The analysis encompasses a realistic scenario where the receiver node is mobile. The obtained system performance represents the guidelines for the design of energy and spectrum-constrained IoT systems with mobile receivers.

As SU-Rx is mobile, the distance between the fixed secondary transmitter and the receiver represents the random variable *r*. It is assumed that the mobile receiver is within maximal distance *D* from the transmitter, i.e. $0 \le r \le D$ and the probability density function (PDF) of distance *r* between SU-Tx and SU-Rx is given by [21]

$$f_r(r) = \sum_{l=1}^{n} \frac{B_l}{D^{\beta_l+1}} r^{\beta_l},$$

where coefficients B_l and β_l, l=1,…,n, that correspond to various topologies of SU movement in one, two or three dimensions are given in [19].
However, the transmit power of the cognitive SU-Tx should not exceed the maximal allowable value

$$P_{SU-Tx,\max} = k_S \frac{Q_p}{\Lambda_S},$$

that guarantees the fulfillment of the interference outage constraint. The coefficient k_S adjusts the transmit power of the secondary user in accordance with the peak interference threshold Q_p and the average value $\Lambda_S = E\left[|g_S|^2\right]$ of the channel power gain in the link from the SU-Tx to the PU-Rx $|g_S|^2$, such that the following maximal tolerable outage probability of primary network $P_{out,PU}$ is not exceeded

$$\Pr\left\{P_{SU-Tx} g_S < Q_p\right\} = 1 - P_{out,PU}.$$

The novel closed-form expressions are derived for the outage probability, the outage throughput and the ergodic capacity of the considered system. Theoretical expressions are verified by using an independently developed Monte Carlo simulation model. Based on the obtained results the influence of the system and channel parameters, as well as interference limitation imposed by the primary network is analyzed.

The dependence of the throughput T_{OUT} on the interference threshold Q_p is analyzed in Figure 14, for two values of the permitted primary network outage probability $P_{out,PU}$ equal 0.1 and 0.01, respectively. The scenarios with different mobility models of the SU-Rx are also considered.

From the obtained results it can be concluded that better system performance is achieved when the permitted outage probability of the PU network is higher. Furthermore, higher throughput values are obtained in the case when the required interference threshold has greater value. With a more lenient condition of harmful interference on the primary receiver, expressed through higher values of the interference threshold and the outage probability of the primary network, a higher value of transmission power is allowed on the SU-Tx. For values of interference threshold higher than 10 dB, the throughput values enter the saturation range and they are not dominantly dependent on the outage probability of the primary network. In this scenario, transmission power of the SU solely depends on harvested energy and not on limitations-caused by harmful interference on the primary user. The throughput values are shown for different mobility models, demonstrating performances in the cases of SU-Rx movement in 1D, 2D and 3D, i.e. along the line path, circle surface or inside the sphere, respectively. It can be noticed that the best results are obtained when movement of SU-Rx can be described using the 1D model path, i.e. when user moves along the line.

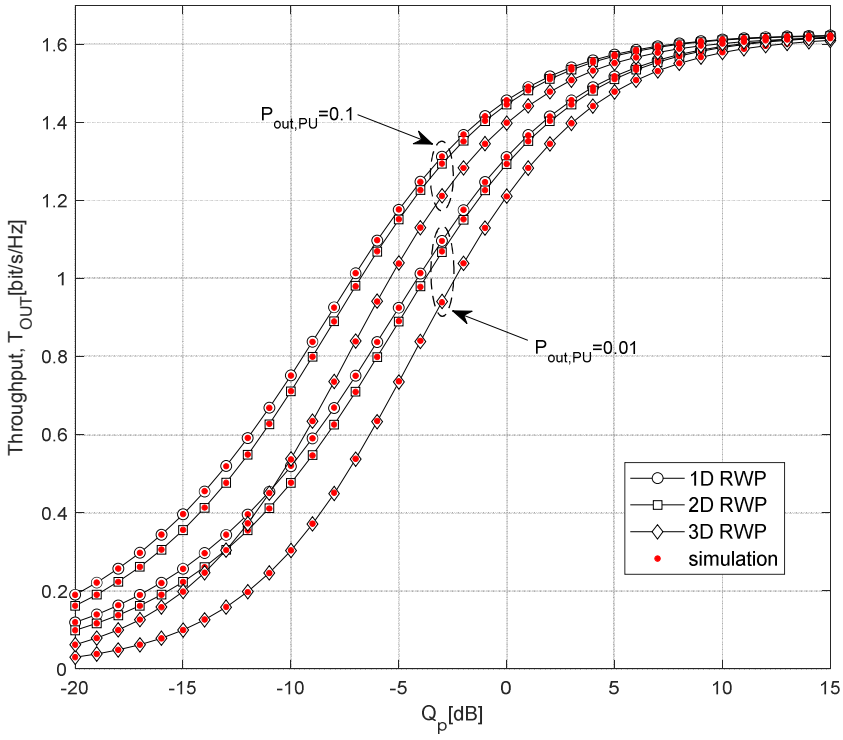

Figure 14. Throughput T_{OUT} vs. interference threshold Q_p, for various mobility models.

SECTION 4 – LOW COMPLEXITY ITERATIVE DECODERS

4.1. LDPC CODES

Belief-propagation (BP) is the state-of-the-art algorithm used for decoding low-density parity-check (LDPC) codes, as provides reasonably good decoding performance on variety of communication channels. The BP decoder is also credited for LDPC codes approaching Shannon capacity on additive white Gaussian noise (AWGN) channel and binary symmetric channel (BSC) [22]. Its hardware-friendly versions are used in communication protocols that involve LDPC codes, like fifth-generation standard for broadband cellular networks (5GNR), or Wi-Fi (IEEE 802.3an) networks. However, drawbacks of BP decoding become visible when applied on short and medium length LDPC codes, as achieved performance is far from maximum-likelihood (ML) performance bounds. This poor behavior of BP decoder is attributed to unavoidable dense structures in Tanner graphs of finite length LDPC codes, generally referred as to trapping sets. Over the years, significant effort was made to identify such structures and to design more resilient decoders. This lead to development of Finite Alphabet Iterative Decoding (FAID) concept that surpasses BP on several regular column weight-3 codes [23]. However, designing a FAID decoder for higher column-weights, or for irregular LDPC codes is challenging, as those codes contain significantly larger variety of trapping sets.

Instead, recent attempts to build superior decoders are oriented to incorporating artificial intelligence concepts into decoder design. Nachmani et al. showed in [24] that the BP decoder represents only a variant of sparse deep neural network (DNN) and that its performance can be improved via training and back-propagation weight updating. The idea was further elaborated by Lugosch and Gross [25] and especially by Xiao et al. [26], where recurrent quantified DNNs are used to design FAIDs that converges faster that BP. However, due to complexity of the proposed DNN framework it is uncertain if it can be extended to longer or higher column-weight codes. In another research direction, DNNs are not used to train the decoder, but rather as a part of the decoding process [28]. Although such decoding schemes can operate beyond BP, their complexity is high, and majority of them are also restricted to very short LDPC codes.

Until recently, bit-flipping decoders were not considered to be competitive to BP decoding (and its simplifications). It has been reported that newly proposed solutions [28]–[31], that emerged from gradient descent bit-flipping decoder (GDBF), originally proposed by Wadayama et al. [32], in some cases perform relatively close to BP decoding on BSC. The GDBF decoder tries to solve the ML decoding problem by using the gradient descent optimization. In each decoding iteration GDBF decoder flips bit vales in order to minimize the ML objective function, i.e., bits with the lowest energy. However, being only an approximation of the ML decoder, the GDBF decoder gets frequently stuck at local optima (trapping sets). It is widely assumed that the optimal way to break trapping set is to insert randomness into decoding process, as the best bit-flipping decoders employ random generators [28]–[31].

It was shown in [33] that probabilistic GDBF (PGDBF) decoder can approach even the ML decoding bound if unbounded number of iterations is allowed. For example, Information Storage Bit Flipping (ISBF) decoder, proposed by Cui et al. [29], defines two flipping thresholds and flips only a portion of randomly chosen bits, with the energy beyond the thresholds. In the most recent publication [31] Savin added the momentum term into the PGDBF energy function and showed that (P)GDBF decoder with momentum ((P)GDBF-w/M) closely approach the floating-point BP decoding performance on BSC. However, the momentum values were chosen empirically, and no method for their selection and optimization is provided. In this paper we propose a novel framework for designing decoders that surpasses the BP decoder on BSC.

In the case of BSC channel, general representation of the inverse energy associated to the *i*-th variable in the *l*-th decoding iteration is given with the expression

$$E^{(l)}(v_i) = \boldsymbol{a}(x_i^{(l)} \oplus y_i) + \boldsymbol{b} \sum_{j \in P(v_i)} s_j^{(l)} - m_l, \quad i = 1, 2, .., N$$

where $\boldsymbol{a} = (a_1,\ldots,a_N)$ and $\mathbf{b} = (b_1,\ldots, b_N)$ are vectors of positive constants, $\boldsymbol{y}$ is the received vector from the channel, $\mathbf{x}^{(l)}$ is a vector of variable estimates from the *l*-th iteration, and corresponding syndrome is defined as $\boldsymbol{s}^{(l)} = \boldsymbol{x}^{(l)} \times \boldsymbol{H}^{\mathsf{T}}$. Variable node v_i is associated with a set of parity equations $P(v_i) = \{j | \boldsymbol{H}_{ji} = 1\}$, where $\boldsymbol{H}$ denotes the parity check matrix, and the cardinality $g_i = |P(v_i)|$ represents the weight of the column that corresponds to the variable v_i. In the above expression, $\boldsymbol{m} = (m_1,\ldots, m_L)$ is a predefined momentum vector that contains non-negative integers sorted in non-increasing order, and l_i is the number of iterations passed from the last flip of the variable v_i.

In our recent paper [34], we have solved a problem of momentum values selection in GDBF-w/M algorithm, by employing genetic algorithm optimization, and constructed the Adaptive Gradient Descent Bit-Flipping Diversity Decoding (AD-GDBF) that outperforms state-of-the-art FAID, PGBFw/M and ISBF decoders. More importantly, for the proposed framework it is immaterial if an LDPC code is regular or irregular, low or high-variable degree or what the code rate is. This - to the best of our knowledge - makes it unique. In addition, the GDBF-w/MA is purely deterministic (does not use random number generators), and for regular codes can be implemented by using only integer arithmetic.

Furthermore, we have shown that performances of the AD-GDBF are beyond the BP decoder on variety of regular and irregular LPDC codes. Due to space limitations we here do not give exact learned momentum and scaling parameter values. Instead, they are publicly available, together with parity check matrices in [35]. We run flooding scheduled BP decoders for 100 iterations, given the fact that further increasing the number of iterations will not significantly influence FER. In Fig. 15(a) we compare the performance of the optimized decoder GDBF w/MA for $L = 300$ iterations, for the Tanner code with N=155, with the BP and FAID decoders. It can be observed that GDBF-w/MA with $L = 300$ outperforms BP in the error-floor region, while increasing the number of iterations to $L = 1000$ enables superior performance compared to 7-level FAID. The GDBF-w/MA decoder with L = 10000 outperforms diversity set of 243 FAID decoders run for more than 29000 iterations. In Fig. 15(b) we examine performance of AD-GDBF on quasi-cyclic column weight 4 regular code called iRISC code, with code rates $R = 0.5$ and lengths $N = 1296$, and compare it with (P)GDBF-w/M and ISBF decoders.

We see that the proposed decoder outperforms concurrent bit-flipping decoders with the same number of iterations. Interestingly, to surpasses BP on code with variable weight 4, GDBF w/MA requires significantly more decoding iterations. In Fig. 15(c) we show performance of code proposed in IEEE 802.3an standard (R = 0.84, N = 2048). It can be observed that for codes with higher code rate GDBF-w/MA surpasses BP with less iterations. Finally, in Fig. 15 (d), we show performance of 5GNR code with N = 1276 and R = 0.75 and validate proposed framework on an irregular code.

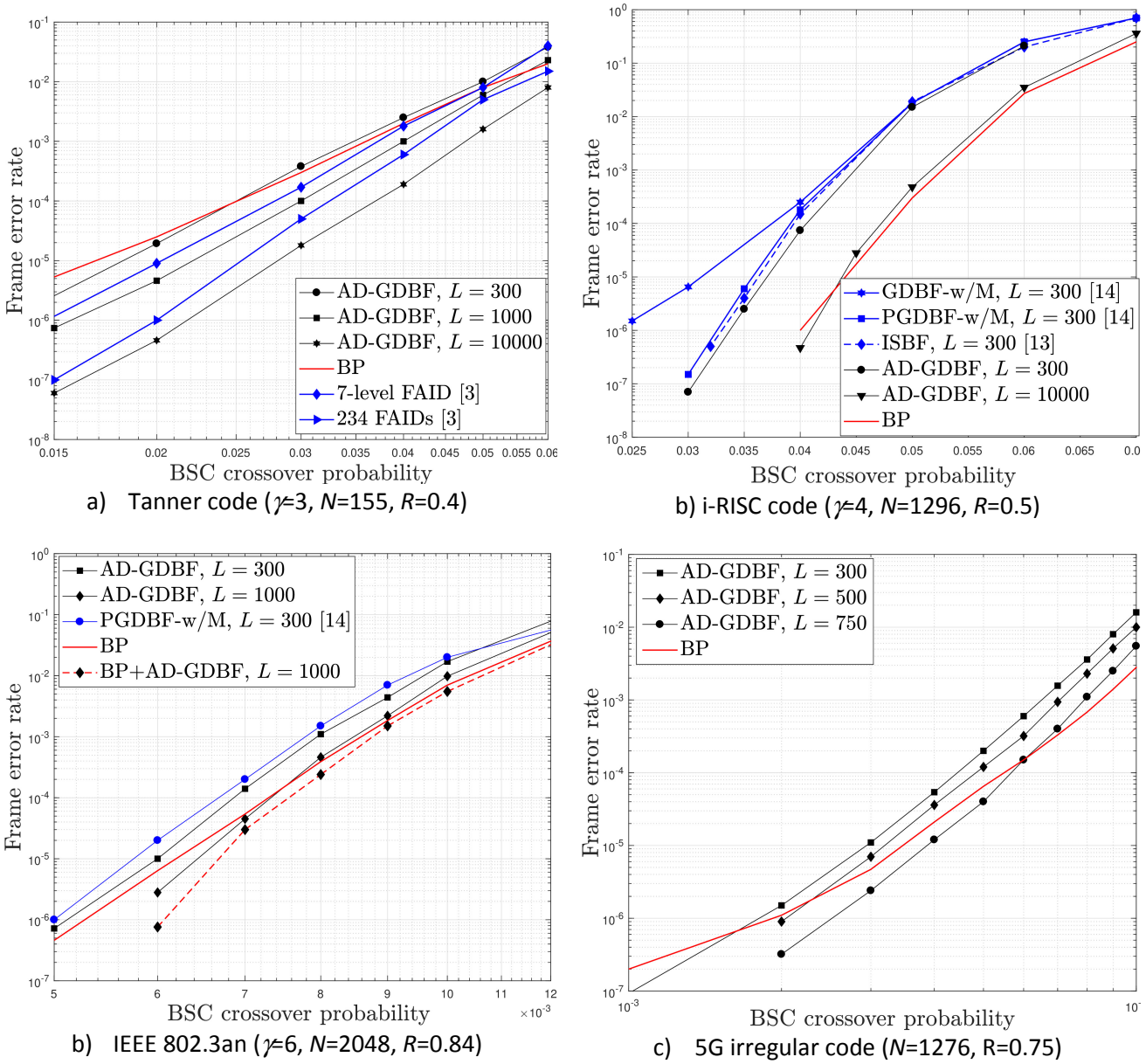

a) Tanner code (γ=3, N=155, R=0.4)

b) i-RISC code (γ=4, N=1296, R=0.5)

b) IEEE 802.3an (γ=6, N=2048, R=0.84)

c) 5G irregular code (N=1276, R=0.75)

Figure 15. Performance of the AD-GDBF decoder on various LDPC codes.

4.1. BCH CODES

In our recent paper [36], we proposed a generalization of the adaptive diversity gradient-descent bit flipping decoder, named generalized AD-GDBF (gAD-GDBF) decoder. While the original AD-GDBF decoder was designed for the binary symmetric channel and used mostly to decode regular LDPC, the gAD-GDBF algorithm incorporates several improvements which make it eligible for the additive white Gaussian channel and decoding of arbitrary linear block code. The gAD-GDBF decoder also uses the genetic algorithm to optimize a set of learnable parameters, for a targeted linear block code. The effectiveness of the proposed method is verified on short Bose–Chaudhuri–Hocquenghem (BCH) codes, where it was shown that for the same number of decoding iterations the gAD-GDBF decoder outperforms the BP decoder in terms of bit error rate and at the same time reduces the decoding complexity significantly.

The detail about the algorithm can be found in paper [36], and here we will propose a performance of the algorithm for some typical BCH codes. The performance of the gAD-GDBF decoder is expressed in a form of the bit error rate (BER) dependency on the Eb/N0 (energy per information bit to noise power spectral density ratio) are presented in Fig. 1 for several BCH codes. The optimized parameters of designed decoders and used parity check matrices are publicly available in [37]. We first verified the significance of the introduced improvements in the gAD-GDBF decoder, by showing its superiority compared to the GDBF-w/M decoder on (63,45) code. Additionally, we observed that the gAD-GDBF decoders, if run for L_{max} = 300 iterations on (63,45) and (127,106) codes provide gain close to 1.0 dB, compared to the BP decoder, run for L_{max} = 50 iterations. Interestingly, our decoders even outperform the BP decoder run for L_{max} = 300. It should be emphasized that increasing the number of iterations for the BP decoder beyond 300, does not improve the decoding, and the performance loss compared to the gAD-GDBF decoder cannot be reduced. Furthermore, we can see that the proposed decoder, run for 300 iterations, outperforms the NBP and NOMS decoders. These decoders are designed only for L_{max} = 5 iterations and it is unknown whether the loss, compared to the gAD-GDBF decoder, can be compensated by adding more iterations. Furthermore, we can see that the gAD-GDBF decoder, run for 25 iterations on (127,106) code, matches the performance of the NOMS decoder for Eb/N0 ≈ 8 dB, while the slopes of the BER curves indicate that the gAD-GDBF decoder will outperform the NOMS decoder, for larger Eb/N0 values.

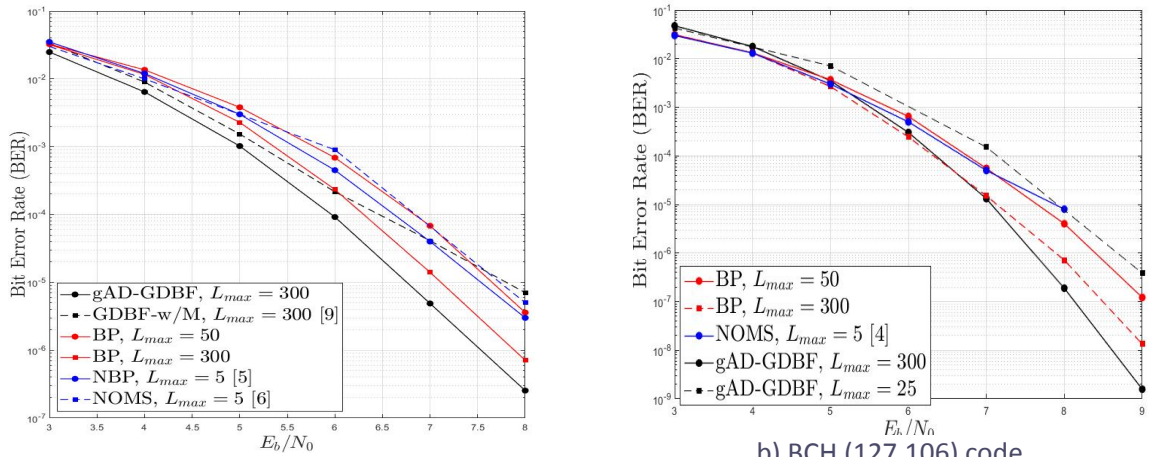

a) BCH (63,45) code

b) BCH (127,106) code

Figure 16. Performance of the gAD-GDBF decoder on various BCH codes.

SECTION 5 – CONCLUSIONS

This Deliverable has presented a review of the techniques that can be applied to increase reliability of the integrated satellite-terrestrial network. A technique based on cooperative relaying is proposed to combine satellite and terrestrial part of the network, to increase the reliability of data transmission. Furthermore, the performance analysis of UAV-assisted wirelessly powered network applicable for industrial IoT and emergency applications is performed. Outage performance of energy limited network with cognitive spectrum utilization and mobile end user is also analyzed. Observed effects can be useful guidelines for the design of various IoT applications. Finally, we have proposed the novel low-complexity algorithm for iterative decoding of linear block codes. The algorithm is based on simple GDBF decoder with momentum, where the momentum vector is optimized by using the adaptation method based on the genetic optimization algorithm. We have validated the performance of our decoder on numerous examples, and have showed its effeteness especially on codes with higher code rates where the proposed algorithm is capable of surpassing significantly complicated BP decoder. The main feature of the proposed solution is possibility to adapt to error patterns specific to a certain LDPC code. Thus, quality of the decoder is mostly influenced by error pattern sets used to train the decoder. We believe that the proposed algorithm could be applied to increase reliability of terrestrial 5G network (where LDPC codes are applied), as well as the satellite networks based on DVB-S2 protocol (where LDPC codes and BCH codes are combined).

REFERENCES

[1] J. N. Laneman, D. N. C.Tse and G. W. Wornell, “Cooperative diversity in wireless networks: Efficient protocols and outage behavior,” *IEEE Trans. Inf. Theory*, vol. 50, no. 12, pp. 3062–3080, 2004.

[2] X. Zhu, C. Jiang, L. Kuang, N. Ge, S. Guo and J. Lu, “Cooperative Transmission in Integrated Terrestrial-Satellite Networks,” *IEEE Network*, vol. 33, no. 3, pp. 204-210, May/June 2019.

[3] V. K. Sakarellos, C. Kourogiorgas, and A. D. Panagopolous, “Cooperative hybrid land mobile satellite-terrestrial broadcasting systems: outage probability evaluation and accurate simulation,” *Wireless Personal Commun*., vol. 79, pp. 1471–1481, November 2014.

[4] G. Pan, J. Ye, J. An, and S. Alouini, “Latency versus Reliability in LEO Mega-Constellations: Terrestrial, Aerial, or Space Relay,” *IEEE Trans. Mobile Comput*., doi: 10.1109/TMC.2022.3168081 (Early Access).

[5] A. Abdi, W. C. Lau, M.-S. Alouini and M. Kaveh, “A new simple model for land mobile satellite channels: first- and second-order statistics,” *IEEE Trans. Wireless Commun*., vol. 2, pp. 519-528, May 2003.

[6] P. Ivanis, D. Drajic, and B. Vucetic, “The second order statistics of maximal ratio combining with unbalanced branches,” *IEEE Commun. Letters*, vol 12, pp. 508-510, July 2008.

[7] V. K.Sakarellos, D. Skraparlis, A. D.Panagopoulos, and J. D. Kanellopoulos, “Cooperative diversity performance of selection relaying over correlated shadowing,” *Physical Commun*., vol. 4, pp. 182–189, March 2011.

[8] J. Milojković, P. Ivaniš, V. Blagojević, S. Brkić, “Performance analysis of land mobile satellite-terrestrial systems with selection relaying", in *Proc. 10th IcETRAN 2023*, TEI 1.2, East Sarajevo, Bosnia and Herzegovina, June 2023.

[9] M. Abramowitz and I. A. Stegun, *Handbook of Mathematical Functions with Formulas, Graphs, and Mathematical Tables*, New York: Dover, 1972.

[10] P. Ivaniš, V. Blagojević, G. Đorđević, “The method of generating shadowed Ricean fading with desired statistical properties”, in *Proc INFOTEH XXII,* Jahorina, BiH, March 2023.

[11] B. Vucetic and J. Du, “Channel modeling and simulation in satellite mobile communication systems,*” IEEE Journal Sel. Areas Commun*., vol. 10, pp. 1209–1218, October 1992.

[12] D. W. Matolak, Q. Zhang and Q. Wu, "Path Loss in an Urban Peer-to-Peer Channel for Six Public-Safety Frequency Bands," *IEEE Wireless Commun. Letters*, vol. 2, no. 3, pp. 263-266, June 2013.

[13] A. Cvetković, V. Blagojević, J. Manojlović, " Capacity Analysis of Power Beacon-Assisted Industrial IoT System with UAV Data Collector ", *Drones*, vol. 7, no. 2, February 2023.

[14] P.K. Sharma, D. Deepthi and D.I. Kim ”Outage probability of 3-D mobile UAV relaying for hybrid satellite-terrestrial networks,” *IEEE Communications Letters*,vol.*24, no.2*, pp.418-422, Febrruary 2020.

[15] Cvetković, V. Blagojević, J. Anastasov, N. T. Pavlović, M. Milošević, “Outage Analysis of Unmanned-Aerial-Vehicle-Assisted Simultaneous Wireless Information and Power Transfer System for Industrial Emergency Applications”, *Sensors*, vol. 23, no. 18, September 2023.

[16] N. Kozić, V. Blagojević, A. Cvetković, P. Ivaniš, "Performance Analysis of Wirelessly Powered Cognitive Radio Network with Statistical CSI and Random Mobility", *Sensors*, vol. 23, no. 9, May 2023.

[17] A. Goldsmith, S. A. Jafar, I. Maric and S. Srinivasa, "Breaking Spectrum Gridlock With Cognitive Radios: An Information Theoretic Perspective," in *Proceedings of the IEEE*, vol. 97, no. 5, pp. 894-914, May 2009.

[18] F. A. Awin, Y. M. Alginahi, E. Abdel-Raheem and K. Tepe, "Technical Issues on Cognitive Radio-Based Internet of Things Systems: A Survey," *IEEE Access*, vol. 7, pp. 97887-97908, July 2019.

[19] J. Jarrouj, V. Blagojevic, P. Ivanis, "Outage Probability and Ergodic Capacity of Spectrum-Sharing Systems with MRC Diversity, " *Frequenz*, vol. 70, no. 3-4, pp. 157-171, 2016.

[20] Camp, T.; Boleng, J.; Davies, V. A survey of mobility models for ad hoc network research. *Wirel. Commun. Mob. Comput.* 2002, 2, 483-502. https://doi.org/10.1002/wcm.72

[21] V. A. Aalo, C. Mukasa, and G. P. Efthymoglou, "Effect of Mobility on the Outage and BER Performances of Digital Transmissions over Nakagami- m Fading Channels," *IEEE Transactions on Vehicular Technology*, vol. 65, no. 4, pp. 2715-2721, April 2016.

[22] T. Richardson, M. Shokrollahi, and R. Urbanke, "Design of capacityapproaching irregular low-density parity-check codes," *IEEE Trans. Inf.Theory*, vol. 47, no. 2, pp. 619–637, Feb. 2001.

[23] D. Declercq, B. Vasić, S. Planjery, and E. Li, "Finite alphabet iterative decoders–part II: Towards guaranteed error correction of LDPC codes via iterative decoder diversity*," IEEE Trans. Commun.,* vol. 61, no. 10, pp. 4046–4057, Oct. 2013.

[24] E. Nachmani, Y. Be'ery, and D. Burshtein, "Learning to decode linear codes using deep learning," in *Proc. 54th Annu. Allerton Conf. Commun., Control, Comput. (Allerton),* Sep. 2016.

[25] L. Lugosch and W. J. Gross, "Neural offset min-sum decoding," in *Proc. IEEE Int. Symp. Inf. Theory (ISIT)*, June 2017.

[26] X. Xiao, B. Vasić, R. Tandon, and S. Lin, "Designing finite alphabet iterative decoders of ldpc codes via recurrent quantized neural networks," *IEEE Trans. Commun*., vol. 68, no. 7, pp. 3963–3974, July 2020.

[27] A. Buchberger, C. Hager, H. Pfistery, L. Schmalenz, and A. Amat, "Learned decimation for neural belief propagation decoders," in *Proc. ICASSP 2021 - 2021 IEEE Inter. Conf. on Acoustics, Speech and Sig. Process. (ICASSP)*, June 2021.

[28] A. Rasheed, O., P. Ivanis, and B. Vasić, "Fault-tolerant probabilistic gradient-descent bit flipping decoder," *IEEE Commun. Letters*, vol. 18, no. 9, p. 1487–1490, Sep. 2014.

[29] H. Cui, L. J., and Z. Wang, "An improved gradient descent bit-flipping decoder for LDPC codes," *IEEE Trans. Circuits and Systems I: RegularPapers*, vol. 66, no. 8, pp. 3188–3200, Aug. 2019.

[30] H. Cui, J. Lin, and Z. Wang, "Information storage bit-flipping decoder for LDPC codes," *IEEE Trans. Very Large Scale Integ. Syst*., vol. 28, no. 11, pp. 2464–2468, Nov. 2020.

[31] V. Savin, "Gradient descent bit-flipping decoding with momentum," in *Proc. 2021 11th Inter. Symp. on Topics in Coding (ISTC)*, Aug. 2021.

[32] T. Wadayama, K. Nakamura, M. Yagita, Y. Funahashi, S. Usami, and I. Takumi, “Gradient descent bit flipping algorithms for decoding LDPC codes,” *IEEE Trans. Commun*., vol. 58, no. 6, p. 1610–1614, June 2010.

[33] B. Vasić, P. Ivanis, D. Declercq, and K. LeTrung, “Approaching maximum likelihood performance of LDPC codes by stochastic resonance in noisy iterative decoders,” in *Proc. 2016 Information Theory and Applications Workshop (ITA 2016)*, Feb. 2016.

[34] S. Brkic, P. Ivanis, and B. Vasić, “Adaptive gradient descent bit-flipping diversity decoding,” *IEEE Commun. Letters*, vol. 26, no. 10, pp. 2257– 2261, Oct. 2022.

[35] “Database of codes and decoders for analysis of AD-GDBF,” https://github.com/brka05/AD-GDBF-decoders.

[36] J. Milojković, S. Brkic, P. Ivaniš, and B. Vasić, "Learning to Decode Linear Block Codes using Adaptive Gradient-Descent Bit-Flipping", in Proc 2023 12th International Symposium on Topics in Coding (ISTC 2023), Brest, France, September 4-8, pp 21-25.

[37] Generalized AD-GDBF decoder database. [Online]. Available: https://github.com/milojko94/gAD-GDBF